Computer Methods and Programs in Biomedicine 213 (2022) 106497

Contents lists available at ScienceDirect

Computer Methods and Programs in Biomedicine

journal homepage: www.elsevier.com/locate/cmpb

Evaluation of cerebrovascular hemodynamics in vascular dementia patients with a new individual computational fluid dynamics algorithm

Jian Xie[a,1], Zaiheng Cheng[b,1], Lihua Gu[a], Bokai Wu[b], Gaojia Zhang[a], Wenshin Shiu[b], Rongliang Chen[b], Zan Wang[a], Chang Liu[b], Jie Tu[c], Xiaochuan Cai[d], Jia Liu[b,*], Zhijun Zhang[a,c,e,**]

[a] Department of Neurology, Key Laboratory of Developmental Genes and Human Disease, Affiliated ZhongDa Hospital, School of Medicine, Institution of Neuropsychiatry, Southeast University, Nanjing, Jiangsu 210009, China
[b] Laboratory for Engineering and Scientific Computing, Institute of Advanced Computing and Digital Engineering, Shenzhen Institute of Advanced Technology, Chinese Academy of Sciences, Shenzhen, Guangdong 518055, China
[c] The Brain Cognition and Brain Disease institute of Shenzhen Institute of Advanced Technology, Chinese Academy of Sciences, Shenzhen, Guangdong 518055, China
[d] Department of Computer Science, University of Colorado Boulder, United States
[e] Research Center for Brain Health, Pazhou Lab, Guangzhou, Guangdong 510330, China

ARTICLE INFO

Article history:
Received 22 June 2021
Accepted 19 October 2021

Keywords:
subcortical vascular dementia
computational fluid dynamics
cerebrovascular hemodynamics

ABSTRACT

Background: Cerebral hemodynamic disorders are involved in the occurrence and progression of vascular dementia (VaD), but the methods to detect hemodynamics remainmultifarious and uncertain nowadays. We aim to exploit a computational fluid dynamics (CFD) approach by static and dynamic parameters, which can be used to detect individual cerebrovascular hemodynamics quantitatively.

Methods: A patient-specific CFD model was constructed with geometrical arteries on the magnetic resonance angiography (MRA) and hemodynamic parameters on ultrasound Doppler, by which, the structural and simulated hemodynamic indexes could be obtained, mainly including the cerebral arterial volume (CAV), the number of visible arterial outlets, the total cerebral blood flow (tCBF) index and the total cerebrovascular resistance (tCVR) index. The hemodynamics were detected in subcortical vascular dementia (SVaD) patients ($n = 38$) and cognitive normal controls (CNCs; $n = 40$).

Results: Compared with CNCs, the SVaD patients had reduced outlets, CAV and tCBF index (all $P \leq 0.001$), increased volume of white matter hyperintensity (WMH) and tCVR index (both $P \leq 0.01$). The fewer outlets ($OR = 0.77$), higher Hachinski ischemic score (HIS) ($OR = 3.65$), increased tCVR index ($OR = 1.98$) and volume of WMH ($OR = 1.12$) were independently associated with SVaD. All hemodynamic parameters could differentiate the SVaD patinets and CNCs, especially the composite index calculated by outlets, tCVR index and HIS (AUC = 0.943). Fewer outlets and more WMH increased the odds of SVaD, which were partly mediated by the tCBF index (14.4% and 13.0%, respectively).

Conclusion: The reduced outlets, higher HIS and tCVR index may be independent risk factors for the SVaD, and a combination of these indexes can differentiate SVaD patients and CNCs reliably. The tCBF index potentially mediates the relationships between hemodynamic indexes and SVaD. Although all simulated indexes only represented the true hemodynamics indirectly, this CFD model can provide patient-specific hemodynamic alterations non-invasively and conveniently.

1. Introduction

Dementia is a disorder characterized by the impairment of cognitive function with attenuated daily activity and psychiatric symptoms, which is the third contributor to neurological disability-adjusted life years (DALYs) [1]. More than 50 million people are affected by dementia globally, it is estimated that the total num-

* Corresponding author.
** Corresponding author at: Department of Neurology, Affiliated ZhongDa Hospital, School of Medicine, Institution of Neuropsychiatry, Key Laboratory of Developmental Genes and Human Disease, Southeast University, Nanjing, Jiangsu 210009, China.
E-mail addresses: jia.liu@siat.ac.cn (J. Liu), janemengzhang@163.com (Z. Zhang).
[1] These authors contributed equally to this work.

https://doi.org/10.1016/j.cmpb.2021.106497
0169-2607/

ber of dementia patients worldwide will reach 82 million by 2030 and 152 million by 2050 [2]. Vascular dementia (VaD) is causing about 15% of dementia cases [3]. The cerebrovascular pathological changes are usually accompanied by intracranial hemodynamic disorder, which is known to be involved in the mechanisms of cognitive decline, particularly for VaD [4]. For instance, patients with cardiac dysfunction manifest hemodynamic disorders and decreased cerebral perfusion, leading to the injury or death of neurons [5,6]. Moreover, remodeling of intracranial or extracranial vessels and increasing resistance of cerebral arteries reduce cerebral perfusion, which impairs the metabolism of brain tissue and the clearance of metabolic substances, such as amyloid-beta ($A\beta$), and further exacerbates the cognitive decline [7–9]. Therefore, the detection of hemodynamic disorders may provide a window to discover potential vascular lesions causing hemodynamic disorder in dementia patients.

The hemodynamic parameters mainly include cerebral blood flow (CBF), cerebrovascular resistance (CVR), flow velocity, fractional flow reserve (FFR) and artery wall shear stress (WSS). Up to now, various imaging methods have been developed and introduced into the measurement of these parameters. Results of transcranial Doppler (TCD) have shown lower velocity of cerebral blood flow and a higher pulsatility index in patients with vascular cognitive impairment, which suggests that increased CVR may contribute to VaD [10]. Similarly, Alzheimer's disease (AD) patients also have mild changes in these parameters [11]. The CBF ratio of gray matter to white matter measured by arterial spin labeling (ASL) also decreases globally in post-stroke dementia patients [12,13], and AD patients exhibit reduced CBF and increased cerebral vascular resistance index (CVRi) in inferior parietal and temporal cerebral regions [14]. Moreover, the 4D flow magnetic resonance imaging (MRI) is an emerging imaging paradigm and capable of quantifying the temporal evolution of complex blood flow patterns, by which AD patients exhibit decreasing mean flow in internal carotid and middle cerebral arteries, which are negatively associated with amyloid levels in cerebrospinal fluid positivity [15].

Until recently, there has been little agreement on the optimal appraisal methods of hemodynamics. First, TCD cannot accurately detect hemodynamic parameters in distal branches of arteries and its accuracy relies on the experience of the operator and the quality of equipment [16]. Second, even though the CBF can be measured by ASL and positron emission tomography (PET), ASL has a low signal-to-noise ratio, and PET is not convenient and widespread in clinical practice, both of them only provide a few hemodynamic parameters [17]. Third, 4D-flow MRI has a trade-off between spatial and temporal resolution, which is suitable for large arteries with fast flows or small vessels with slow flows. Moreover, the time-consuming characteristic impedes its spread [18]. Therefore a multifunctional, non-invasive and accurate measurement of cerebral hemodynamics is necessary for clinical use.

Computational fluid dynamics (CFD) is an alternative method of the abovementioned imaging, and it provides detailed hemodynamic parameters of patients non-invasively [19]. Several CFD approaches using routinely available medical images have been used to detect hemodynamic properties, e.g., FFR in the coronary artery can be estimated non-invasively with CFD from computed tomography angiography (CTA) images, which is highly comparable with the FFR measured by an interventional pressure wire [20,21]. Moreover, the rupture risk and pressure of the intracranial aneurysm can be assessed with CFD, thereby improving the understanding of the biomechanics of the aneurysms [22]. In our previous pilot study, the fractional pressure ratios assessed by CFD are comparable with results of digital subtraction angiography (DSA) [23]. Therefore CFD avoids unnecessary interventional angiography effectively and has considerable application prospects. However, the boundary conditions of previous models based on uniform parameters of the vascular inlets [24], and the individual difference was underestimated. Therefore a CFD model constructed by individual physiological parameters may become an accurate method to quantify cerebral hemodynamics.

To overcome the limitations of non-specificity, the present study used in-house CFD software to quantify and visualize the hemodynamic properties and indexes of arterial structure. The whole cerebral arteries were visualized on the reconstructed arterial graphs, and boundary parameters of inlets were derived from vascular Doppler. To the best of our knowledge, the CFD model has not been applied to detect hemodynamic alterations in dementia patients. Thus this study aimed to explore whether this CFD model can differentiate the hemodynamic alterations between patients with SVaD and CNCs, and further reveal the potential mechanisms of the occurrence and progression of SVaD.

2. Methods

2.1. Participants

The present cross-sectional study included SVaD patients ($n = 38$), and cognitive normal controls (CNCs) ($n = 40$). The diagnosis of probable SVaD accorded to the criteria of Guidelines from the Vascular Impairment of Cognition Classification Consensus Study (VICCCS) and Mini-Mental State Examination (MMSE) score$<$ 24. Meanwhile, the typical pathological changes of SVaD include subcortical infarcts (lacunes) and white-matter lesions. Participants were recruited in the control group according as follow. First, they did not report any cognitive impairment, neurological symptoms or heavy systemic disease. Second, participants did not show any neurological signs according to physical examinations. Third, The CNCs did not suffer from stroke or other cerebrovascular diseases, except for the asymptomatic lacunar infarct basing on MRI and magnetic resonance angiography (MRA). Subjects were excluded from this study if they suffered from other definite causes of dementia. This study was approved by the ethics committee of the Affiliated ZhongDa Hospital, Southeast University (2019ZDSYLL189-P01).

2.2. Collection of demographic data

All participants underwent comprehensive examinations, including physical examination, medical evaluation, Hachinski ischemic score (HIS), blood draw, Doppler ultrasonography of the cervical arteries and MRI + MRA. The measurement of blood pressure by electronic sphygmomanometer was arranged before examination of cervical arteries ultrasonography. The systolic blood pressure (SBP) and diastolic blood pressure (DBP) were recorded. Mean arterial pressure (MAP) was calculated using the formula: MAP = DBP + (SBP - DBP)/3.

2.3. Protocols of imaging

Doppler ultrasonography was performed to measure velocities of the blood flows of the left and right internal carotid arteries (ICA) and vertebral arteries (VA) using high-resolution ultrasound (LOGIQ E9 system, GE Healthcare, Waukesha, WI, USA) at 8–15 MHz. Peak systolic velocity (PSV) and end diastolic velocity (EDV) were used to set up boundary conditions of the CFD model. All participants underwent MRI and MRA scanning using a 3.0 T MRI scanner (Magnetom Verio, Siemens Healthcare, Erlangen, Germany) with a 12-channel head coil at the Department of Radiology, Affiliated ZhongDa Hospital, Southeast University. The MR sequences included T1-weighted imaging (T1WI), T2-weighted imaging (T2WI), and MRA. The above imaging sequences were applied with the parameters as follows: (1) T1WI: repetition time (TR),

700 ms; echo time (TE), 26 ms; number of excitations (NEX), 2; slice thickness, 0.6 cm. (2) T2WI: TR, 2800 ms; TE, 50 ms; NEX, 4; slice thickness, 0.6 cm. (3) TOF (Time of Flight)-MRA: TR, 21.0 ms; TE, 3.6 ms; flip angle, 25; NEX, 1; field of view, 200 × 160.4 mm; matrix size, 216 × 384; slice number, 150; and slice thickness 0.7 mm.

2.4. Measurement of subject-specific hemodynamic parameters with CFD

2.4.1. Image processing and CFD mesh generation

MRA images were exported from the MRI scanner in the standard Digital Imaging and Communication in Medicine (DICOM) format. The cerebral artery was segmented from each DICOM image using 3D region-growing provided by Mimics software (materialize NV, Belgium), and the results were inspected and refined by two radiologists independently. The 3D geometry of the cerebral artery was then reconstructed, by which, structural indexes could be calculated by Mimics, including the number of outlets and volume of cerebral arteries. The computational domain of CFD was discretized by a mesh generated by ANSYS ICEM CFD software (ANSYS, Inc., USA). Due to the complexity of the geometry, an unstructured tetrahedral mesh was used. The total number of elements was greater than 1 million and a minimum elemental volume of approximately 1.0×10^{-8} cm^3, which is used to capture the detailed features of the flow dynamics of the blood flow, especially near the area of artery with stenosis.

2.4.2. Modeling blood flow

The blood flow was assumed to be a vicious and incompressible Newtonian fluid, the heat transfer and compressibility effects of the vascular wall were neglected in this process. The blood flow was characterized by a constant density $\rho = 1.06 \times 10^3 kg.m^{-1}$ and a dynamic viscosity $\mu = 3.5 \times 10^{-3} kg.m^{-1}.s^{-1}$ [25,26]. A typical carotid artery has a diameter $D = 6.0 \times 10^{-3}$ m and the velocity of blood flow is around $v = 0.4\ m.s^{-1}$, as a result, the Reynolds number: $Re = \rho vD/\mu \approx 121$, which suggests that the blood flow was laminar. An unsteady incompressible Navier-Stokes equation was utilized to describe the blood flow, as follows:

$$\frac{\partial \mathbf{v}}{\partial t} + (\mathbf{v} \cdot \nabla)\mathbf{v} = -\frac{1}{\rho}\nabla p + \frac{\mu}{\rho}\nabla^2 \mathbf{v} + \mathbf{f}, \tag{1.1}$$

The equation for conservation of mass was defined as:

$$\nabla \cdot \mathbf{v} = 0, \tag{1.2}$$

where $\mathbf{v}$ is the velocity vector, p is the pressure, and $\mathbf{f}$ is the body force, assumed to be 0.

To solve Eqs. (1.1) and (1.2), a finite volume method using ANSYS CFX software version 14.5 (ANSYS, Inc., USA) was used. CFD simulations were conducted on an AMAX server with dual 22-core Intel Xeon E5–2699 v4 CPUs running at 2.20 GHz with 256 GB memory. The computational mesh was partitioned using a *k*-way Metis algorithm with a message passing interface (MPI) for the communication among the processor cores. The blood flow for a 5 s period in each cerebral artery was simulated with a time step size of 0.01 s. A second-order backward Euler scheme was used for the transient term. The criteria for convergence was set such that the initial root mean square error (RMSE) was reduced by a factor of 1.0×10^{-5}.

2.4.3. Determination of boundary conditions

Both PSV and EDV measured at the inlets of the ICA and the VA were used to estimate the respective mean velocity, defined as $V_{mean} = \frac{1}{3}V_{PSV} + \frac{2}{3}V_{EDV}$, which was assumed to be present at the centerline of the vessels. The flow was assumed to be laminar with pulsatility neglected at all inlets. The flow rate at the inlet was approximated by $Q_{in} = \frac{1}{2}V_{mean} \cdot A_{in}$, where A_{in} was the cross-sectional area of the artery at the inlet. The velocity profile was assumed to be parabolic with zero value on the wall of the artery [27]. The cross-sectional area was calculated by $A_{in} = \pi \cdot (\frac{D_{in}}{2})^2$, where D_{in} is the diameter of the inlet, measured from the MRA images. The tCBF index was calculated by the sum of the flows from the internal carotid and the vertebral Q_{in}. For the outlets, a resistive boundary condition was applied to mimic the downstream resistance, assumed to be inversely proportional to the diameter of the outlet. The tCVR index R_{Total} was calculated from the total inflow $Q_{total} = Q_{in}^{ICA} + Q_{in}^{VA}$ and the MAP, approximated by the brachial blood pressure, that was $R_{total} = MAP/Q_{total}$. R_{out} at each outlet was derived from R_{total} and the diameter of the outlet. Finally, the outlet pressure P_{out} was calculated by $P_{out} = Q_{out} \bullet R_{out}$, where Q_{out} is the flow rate at each outlet and estimated from the area integral of the outlet velocity V_{out}. The scheme used to set the boundary conditions is shown in Fig. 1, and hemodynamic parameters in arteries larger than 0.2 cm in diameter could be estimated by the CFD model.

2.5. Statistical analysis

Statistical analyses were performed using SPSS version 25.0 (IBM Corp., Armonk, NY, USA). The normality of the data distribution was assessed by the Shapiro-Wilk test. The homogeneity of variance in all variables with normality was assessed by Levene's test. Continuous variables with normal distribution were presented as mean ± standard deviation (SD), non-normal variables were reported as median (interquartile range; IQR), categorical data were expressed numerically. Mean values of two continuous normally distributed variables were compared by independent samples Student's test. The Mann-Whitney *U* test was used to analyze the statistical significance of differences in variables with nonnormal distribution or heterogeneity of variance. Chi-Square (χ^2) test was used to compare categorical data. Pearson or Spearman correlations were used to examine the associations of hemodynamic parameters and structural indexes. To elucidate the independent contributions of hemodynamic parameters to dementia, binary logistic regression analyses were performed across the SVaD patients and CNCs groups. Results are expressed as odds ratios (*OR*) and corresponding 95% confidence intervals (95% CI), which were used to interpret the effect of independent variables on "dementia". To evaluate the diagnostic accuracy, the abilities of hemodynamic parameters to differentiate SVaD and CNCs were assessed by the area under the receiver operator characteristic curve (ROC). Propensity score matching with 1:2 was applied to pair two groups at baseline (i.e., age) with the plug-in components (PSMATCHING3.04.spe) in SPSS, in which, the caliper of a width of 0.2 was used [28].

Mediation analysis was performed with the SPSS PROCESS macro (version 3.5) [29]. Given the injuries of pathological factors to dementia are mediated by CBF, we examined the one mediator path (PROCESS Model (4): outlets to tCBF index to SVaD, CAV to tCBF index to SVaD, and tCVR index to tCBF index to SVaD. Moreover, a multiple mediator path (PROCESS Model 6) was used to determine whether the tCVR index and tCBF index mediate the association between the volume of white matter hyperintensity (WMH) and SVaD. Mediation analyses incorporated age, sex as covariates. A p-value less than 0.05 was deemed statistically significant.

3. Results

3.1. Comparison of baseline demographic and clinical characteristics between two groups

The baseline demographic and clinical data of the 78 included participants was summarized in Table 1. As compared to CNCs, the

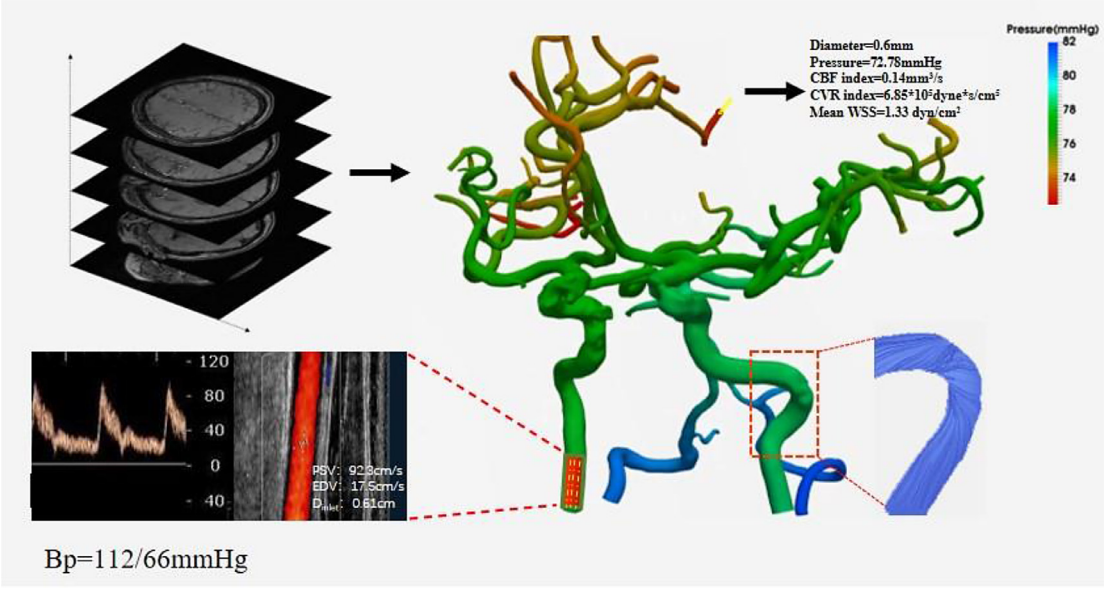

Fig. 1. The reconstructed pseudo-color map shows the vascular pressures of different arteries. This CFD model constructed by MRA, in which the patient-specific hemodynamic parameters derived from Doppler and mean arterial pressure were used to be boundary conditions. By which the parameters of any part of arteries or distal branches can be calculated.

Table 1
Demographics and clinical characteristics.

Characteristics	SVaD (n = 38)	CNCs (n = 40)	t value	P value
Sex(male)	25	20	χ^2= 1.99	0.158
Age (year), media (IQR)	83.00 (75.75,85.50)	75.5 (73.00,78.75)	Z = - 3.54	<0.001
BMI	23.72 ± 3.36	25.12 ± 3.37	1.74	0.086
SBP (mmHg)	139.03 ± 17.49	138.80 ± 17.09	- 0.06	0.954
DBP (mmHg)	76.74 ± 13.27	73.48 ± 9.96	- 1.22	0.222
History of hypertension	24	32	χ^2= 2.73	0.161
History of diabetes	15	8	χ^2= 3.55	0.060
History of asymptomatic lacunar	18	12	χ^2= 2.48	0.115
History of hyperlipemia	2	4	χ^2= 0.13	0.791
Smoking history	4	8	χ^2= 0.71	0.398
History of CHD	6	6	χ^2= 0.01	0.923
TC (mmol/L)	4.06 ± 1.06	4.34 ± 1.02	1.150	0.254
GTs (mmol/L)	1.20 ± 0.76	1.60 ± 1.12	1.82	0.073
HDL (mmol/L)	1.17 ± 0.38	1.26 ± 0.28	1.19	0.240
LDL (mmol/L)	2.38 ± 0.87	2.41 ± 0.74	0.14	0.889
ALT (U/L)	25.45 ± 24.91	18.03 ± 11.99	- 1.67	0.099
UN (mmol/L)	6.50 ± 3.61	5.65 ± 1.65	- 1.34	0.184
HbA1c%, media (IQR)	6.00 (5.57,7.57)	5.75 (5.40,6.58)	Z = - 1.29	0.197
Shcy (μmol/L)	14.93 ± 10.68	19.21 ± 9.14	1.755	0.084
Volume of WMH (cm^3), media(IQR)	24.37 (13.21,34.77)	4.83 (1.68,9.67)	Z = - 4.70	<0.001
HIS, media (IQR)	7 (4, 9)	2 (2,3)	Z = - 5.74	<0.001

Abbreviation: ALT: alanine aminotransferase, BMI: body mass index, CHD: coronary heart disease. DBP: diastolic blood pressure, GT: triglycerides, HbA1c: Hemoglobin A1c, HIS: Hachinski ischemic score, HDL: high-density lipoprotein, IQR: interquartile range, LDL: low-density lipoprotein, SBP: systolic blood pressure, Shcy: serum homocysteine, Tc: total cholesterol, UN: urea nitrogen, WMH: White matter hyperintensity.

average age of SVaD patients (Z = - 3.54, P < 0.001) was older. The SVaD participants had a significantly increased volume of WMH (Z = - 4.70, P < 0.001) and HIS (Z = - 5.74, P < 0.001). There were no significant differences in other baseline data between the two groups(all P > 0.05). After performed propensity score matching for age, the increased volume of WMH and HIS were found in SVaD patients yet (Supplementary Table 1).

3.2. Comparison of hemodynamic parameters between groups

Two typical examples of the color maps of pressure and velocity throughout the arterial tree are displayed in Fig. 2 for each group. The hemodynamic parameters of all subjects were calculated by the 3D CFD model (Tables 2 and S3). As compared with CNCs, SVaD patients had a reduced number of outlets, CAV and tCBF index (all $P \leq 0.01$). On the contrary, there was a significantly increasing tCVR index in SVaD group (P < 0.001). Using age-matched subjects, all hemodynamic parameters mentioned above also shown significant differences between the two groups (Supplementary Table 1).

3.3. Binary logistic regression analysis and ROC curve analysis

Binary regression analysis demonstrated that a fewer number of outlets were independently associated with SVaD (OR = 0.77; 95%CI: 0.65–0.92). The increasing tCVR index (OR = 1.98, 95%CI: 1.16–2.28), the volume of WMH (OR = 1.12, 95%CI: 1.03–1.2 2) and HIS (OR = 3.65, 95%CI: 1.58–8.43) were independently related to SVaD (Table 3). On regression analysis of age-matched subjects, all

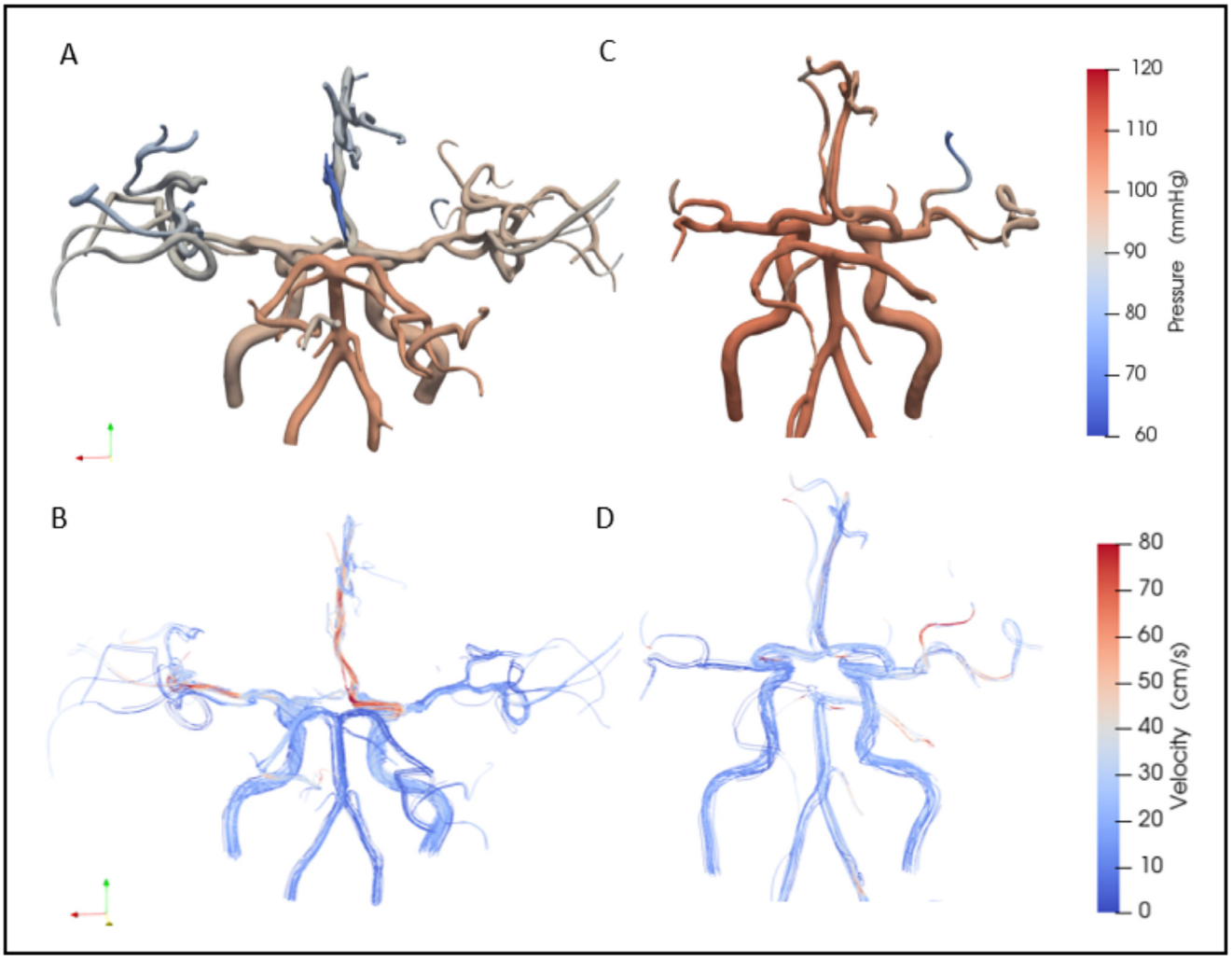

Fig. 2. Two typical examples of pressure distribution and streamlines of blood flow velocity. The first column (A and B) is for a cognitive normal subject, the second column (C and D)is for a SVaD patient. According to computation, the total blood flow index in the models 998 ml/min (cognitive normal subject) and 725 ml/min (SVaD patient), respectively.

Table 2
Arterial structure characteristics and hemodynamic parameters.

Hemodynamic parameters	SVaD (n = 38)	CNCs (n = 40)	t value	P value
Number of outlet	31.18 ± 7.39	44.20 ± 11.12	Z = - 5.09	< 0.001
CAV (cm^3)	10.29 ± 2.66	12.35 ± 2.71	3.38	0.001
tCBF index (cm^3/s)	9.65 ± 3.04	12.12 ± 2.42	3.97	< 0.001
tCVR index ($dyne^*s/cm^5$)	11,844.90 ± 4739.08	9280.57 ± 2239.75	Z = - 2.55	0.01

Table 3
Binary logistic regression analysis for hemodynamic parameters.

Independent variables	SVaD vs CNCs β	P (Sig)	OR (95% CI)
Number of outlet	- 0.263	0.003	0.77 (0.65–0.92)
tCVR index (^{*1000} $dyne^*s/cm^5$)	0.685	0.012	1.98 (1.16–2.28)
HIS	1.295	0.002	3.65 (1.58–8.43)
Volume of WMH (cm^3)	0.110	0.013	1.12 (1.03–1.22)

four variables were independent risk factors (Supplementary Table 2). The ROC curves showed that all hemodynamic parameters have significantly higher discriminative power to distinguish SVaD and CNCs, especially the composite index of outlets, tCVR index and HIS (AUC = 0.943, Fig. 3).

3.4. The correlation analysis and mediation analysis of hemodynamic parameters

Bivariate Spearman rank correlation showed that the CAV was positively correlated with the number of outlets (All P < 0.001; Fig. 4A) in all groups. The tCBF index was negatively associated with the tCVR index in two groups ($r_{s\text{-}SVaD}$= - 0.760, P < 0.001; $r_{s\text{-}CNCs}$= - 0.746, P < 0.001; Fig. 4B). Even though there were significant differences in age and volume of WMH between the two groups, correlation analyses revealed that the tCBF index did not relate to age or volume WMH (Fig. 4C and 4D, both P > 0.10).

Based on the results mentioned above, mediation analyses were performed to examine the hypothetic pathways. The percentage of the total effect of outlets' number on the SVaD that was mediated through tCBF index was 14.4% (Fig. 4E). The reduced CAV and increased tCVR index had potential effects on SVaD, which

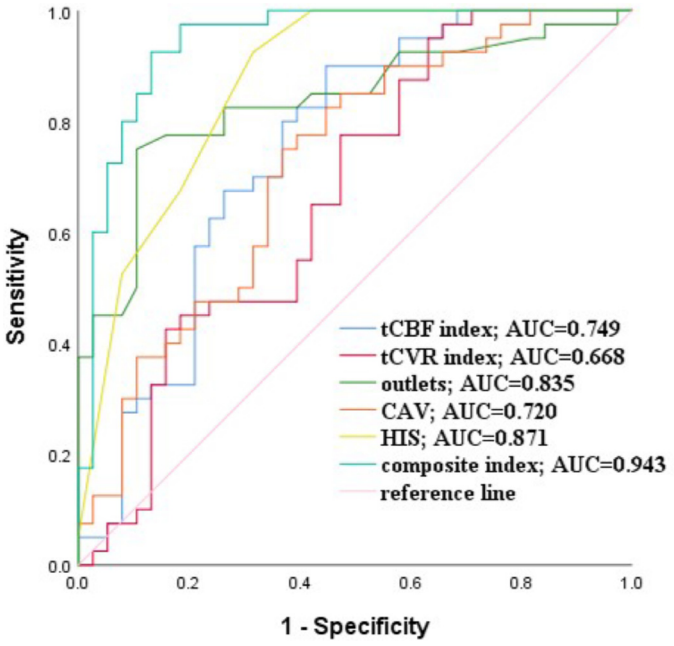

Fig. 3. The ROC of the ability of hemodynamic parameters to differentiate between CNCs and SVaD. The composite index was predicted probability that were calculated by binary logistic regression with all hemodynamic parameters and Hachinski ischemic score. The variables in final step of binary logistic regression included outlets, tCVR index and Hachinski ischemic score. The predicted probability is $P = [exp(-2.98–0.13 \times X_1 + 0.37 \times X_2 + 1.00 \times X_3)]/[1 + exp(-2.98–0.13 \times X_1 + 0.37 \times X_2 + 1.00 \times X_3)]$, X_1 is the number of outlets, X_2 is tCVR index(1000 *dyne*s/cm 5), X_3 is Hachinski scale.

were totally mediated by the tCBF index (Fig. 4F and 4G). A serial 2-mediator analysis demonstrated that more volume of WMH increased the risk for SVaD, which was partly mediated by tCVR index through tCBF index (Ration indirect = 13.0%, $P < 0.001$. Fig. 4H).

4. Discussion

In the present study, we developed a novel 3D CFD approach to measure the changes in hemodynamics and visible arteries in patients with SVaD quantitatively for the first time. The main findings are summarized as follows. First, as compared with CNCs, SVaD groups had more WMH, higher HIS, increased tCVR index, reduced visible arterial volume or outlets and tCBF index. Even though there was a significant difference in baseline age of the two groups, the differential hemodynamic indexes in unmatched analyses also existed in the results of age-matched univariate analysis. Second, the independent risk factors of SVaD included increased tCVR index, higher HIS, more volume of WMH and less visible arterial outlets. Third, all hemodynamic parameters and Hachinski ischemic score had discriminative power to differentiate SVaD and CNCs, especially the composite index calculated by outlets, tCVR index and HIS. Fourthly, the CAV was positively associated with the number of outlets, and the tCBF index was negatively related to the tCVR index in all subjects. On the contrary, there were not any relationships between the tCBF index and age or WMH. Finally, fewer outlets increased the odds of SVaD, which was partially mediated by the tCBF index. However, the proportion of SVaD risk explained by the CAV or tCVR index was totally mediated by the tCBF index. The augmented volume of WMH increased the risk for SVaD, some of this relationship may be mediated by the tCVR index through the tCBF index.

It is challenging to measure hemodynamic parameters directly. Basing on our previous study with CTA [23], a novel patient-specific CFD model was constructed by MRA and ultrasonic flow parameters. This approach has several attractive features. First, it is more specific and convinced than other CFD models based on the uniform parameters of inlets from the healthy subject. Second, it is non-invasive and non-radioactive. Meanwhile, the imaging of CTA and DSA can be used to replace MRA, thus improving the accessibility to most medical centers. Third, the model has a high spatial resolution, intracranial arteries with a diameter larger than 2 mm can be evaluated, allowing hemodynamic parameters of the distal branches to be available. Fourthly, comprehensive hemodynamic parameters can be acquired in the CFD model conveniently, such as tCBF indexes, tCVR indexes, velocity, FFR, CAV and arterial WSS [30]. Hence there is a need for expanding the application of these parameters in other cerebrovascular diseases. It is worth mentioning that all simulated indexes calculated by this CFD only represented the real ones indirectly, and all indexes can be used to differentiate between normal and abnormal hemodynamics, but not be equivalent to the real value measured with invasive methods. Moreover, the true physiological meanings of hemodynamic parameters need more following researches to verify.

In this study, SVaD patients revealed that less tCBF index and increased tCVR index. While undertaking the cognitive task, healthy subjects and stroke patients exhibited a significant increase in CBF and bloodstream velocity [7,31], which suggested that cerebrovascular circulation adjusts its hemodynamic response to metabolic requirements. Previous researches have shown that the CBF of the frontal and parietal cortex decreased in SVaD patients [32]. Moreover, the CVRi correlated positively with the severity of dementia [33]. Therefore, the tCBF index and tCVR index may play a critical role in the progression of SVaD.

In our study, patients with SVaD had decreasing visible outlets and CAV, and the CAV was positively related to the outlets in all subjects. The mechanism of 3D TOF MRA relies on inflow-based techniques [34]. To some extent, both the arterial outlets and volume reflect the internal diameters of arterial branches. Therefore, the CAV and outlets may exacerbate the occurrence of SVaD mediated by the tCBF index totally or partly.

Stabilized CBF not only depends on cerebral arteries structure but also heart function and resistance [6]. In the present study, the tCBF index was significantly and negatively correlated with the tCVR index, and the tCBF index might be mediated the effect of the tCVR index on SVaD totally. All the above results confirmed that abnormal arterial structure and hemodynamic parameters might affect the perfusion of the whole brain and the progression of SVaD. Early detection of abnormal hemodynamics may help clinicians became more aware of latent pathological changes of structure and function in the neurovascular unit.

In the present study, patients with SVaD showed an increased volume of WMH, which is an independent risk factor for SVaD. Previous studies have verified that WMH is a pathological factor of SVaD, which participate in the development and progression of SVaD [35]. Furthermore, we found that the effect of extensive WMH on SVaD was partly mediated by a higher tCVR index and lower tCBF index. Consequently, the pathological changes of small vessels may downregulate cerebral perfusion, but there must be other mechanisms that deteriorate the progress of SVaD.

In the present study, the HIS also showed a higher capability to distinguish SVaD and CNCs. Moreover, the predicted probability calculated by HIS, tCVR index and outlets further enhanced the accuracy in the differential diagnosis of SVaD. HIS is a frequently-used and available scale to differentiate the SVaD patient. Using postmortem neuropathologic examination, the sensitivity and specificity of HIS were 0.69 and 0.92, respectively [36]. Therefore, the application of CFD would provide a new noninvasive method to aid the diagnosis of SVaD even though additional time and economic cost.

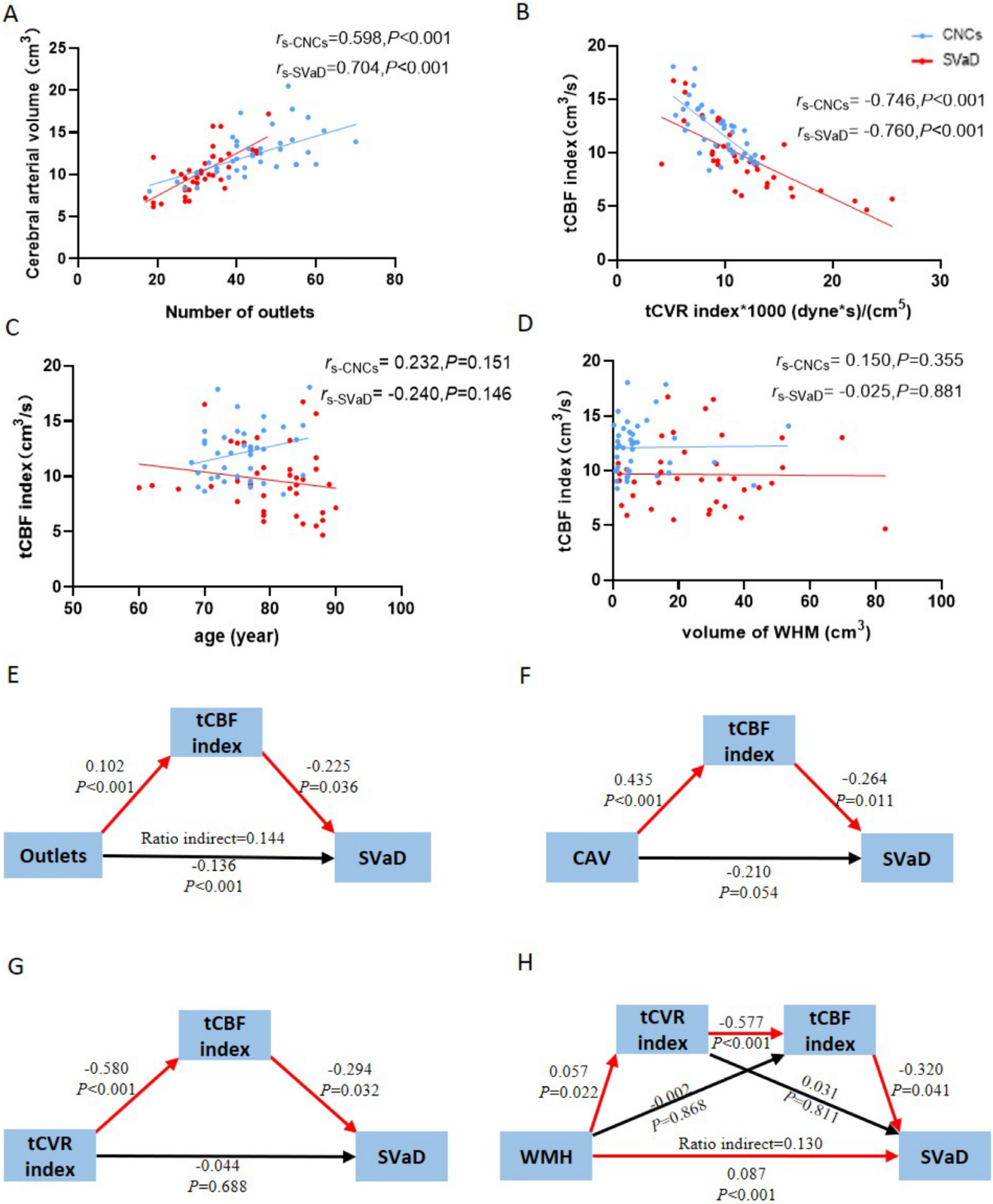

Fig. 4. The CAV was positively associated with the number of outlets in two groups (A, both $P < 0.001$). The tCBF index was negatively related with tCVR index in both group (B, $P < 0.001$), instead of age or volume of WMH (C and D, both $P > 0.05$). Mediation analysis demonstrated that tCBF index could be a mediator of the association between outlets and SVaD (E), tCBF index totally mediated the effect of CAV or tCVR index on SVaD (F and G), The percentage of the total effect of WMH on the SVaD was mediated through tCVR index and tCBF index was 13.0% (H).

Several limitations of this study should be mentioned. First, this study is a cross-sectional study, and the correlation between hemodynamic parameters and SVaD need to be verified by follow-up studies. Second, this study has only been carried out with a small sample size, which may weaken this study's findings, especially the mediation analysis. Therefore large-scale clinical studies are warranted for further verification of the results or conclusions of this study. Third, even though the values of MAP in major arteries were equal, the MAP calculated with the traditional one-third rule underestimated the real MAP by nearly 5.0 mmHg [37]. Therefore, the automated oscillometric devices would be better substitutes for the traditional way, especially in the MAP [38]. Finally, the simple resistance outlet boundary condition we have chosen in the present study was different from our previous work [23], in which, a Windkessel boundary condition which accounts for arterial compliance in the distal vessels can achieve more realistic wave reflection in the simulation. However, in the present study, we focused on static hemodynamic parameters, e.g., tCBF index and tCVR index. The results from these two types of boundary conditions are comparable for these static parameters.

5. Conclusion

The independent risk factors of SVaD include fewer cerebral arterial outlets, higher HIS, increased tCVR index and volume of WMH. The abnormal hemodynamic parameters can be used to differentiate the SVaD patient and CNCs, especially the predicted probability calculated by HIS, number of outlets and tCVR index. The tCBF index totally mediated the effect of CAV or tCVR index on SVaD and partially mediated the relationships between SVaD and WMH or arterial outlets. With the verification of prospective clinical trials, this CFD model will provide clinicians with methods to discover and monitor latent neurovascular dysfunction in patients with SVaD.

Availability of data and material

Data are available upon reasonable request.

Funding

This research was supported by grants from the National Natural Science Foundation of China (81830040, 82130042 to ZJZ), the National Key Research and Development Plan of China (No. 2016YFC1306700 to ZJZ), Science and Technology Program of Guangdong (2018B030334001 to ZJZ), Program of Excellent Talents in Medical Science of Jiangsu Province (JCRCA2016006 to ZJZ). National Natural Science Foundation of China (81661168015, 61703017, 81871447 to JL), and Shenzhen Science and Technology Innovation Commission (ZDSYS201703031711426 to JL). The funding bodies had no role in the study's design, data collection, analysis, interpretation, or writing of the manuscript.

Ethical standards

This study was approved by the ethics committee of the Affiliated ZhongDa Hospital, Southeast University. Written informed consent was obtained from each participant.

Declaration of Competing Interest

None of the authors have any conflicts of interest or financial ties to disclose.

CRediT authorship contribution statement

Jian Xie: Formal analysis, Data curation, Visualization, Writing – original draft, Writing – review & editing. **Zaiheng Cheng:** Visualization, Writing – review & editing. **Lihua Gu:** Data curation, Writing – review & editing. **Bokai Wu:** Visualization, Software, Writing – review & editing. **Gaojia Zhang:** Data curation, Writing – review & editing. **Wenshin Shiu:** Methodology, Writing – review & editing. **Rongliang Chen:** Methodology, Writing – review & editing. **Zan Wang:** Data curation, Writing – review & editing. **Chang Liu:** Visualization, Writing – review & editing. **Jie Tu:** Writing – review & editing. **Xiaochuan Cai:** Methodology, Methodology, Writing – review & editing. **Jia Liu:** Visualization, Formal analysis, Data curation, Writing – original draft, Writing – review & editing. **Zhijun Zhang:** Visualization, Formal analysis, Data curation, Writing – review & editing.

Acknowledgments

We would like to express our thanks to all participants in this study, without whose support this research would not have been possible to be finished. We thank the colleagues who participated in the collection of clinical data.

Supplementary materials

Supplementary material associated with this article can be found, in the online version, at doi:10.1016/j.cmpb.2021.106497.

References

[1] GBDN Collaborators, Global, regional, and national burden of neurological disorders, 1990–2016: a systematic analysis for the global burden of disease study 2016, Lancet Neurol. 18 (5) (2019) 459–480, doi:10.1016/S1474-4422(18)30499-X.
[2] C. Patterso, World Alzheimer's report 2018-the state of the art of dementia research: new frontiers. 2018, London.
[3] J.T. O'Brien, A. Thomas, Vascular dementia, Lancet 386 (10004) (2015) 1698–1706, doi:10.1016/S0140-6736(15)00463-8.
[4] R. Wang, L. Fratiglioni, G. Kalpouzos, et al., Mixed brain lesions mediate the association between cardiovascular risk burden and cognitive decline in old age: a population-based study, Alzheimer Dement. 13 (3) (2017) 247–256, doi:10.1016/j.jalz.2016.06.2363.
[5] R.A.H. Stewart, C. Held, S. Krug-Gourley, et al., Cardiovascular and lifestyle risk factors and cognitive function in patients with stable coronary heart disease, J. Am. Heart Assoc. 8 (7) (2019) e010641, doi:10.1161/JAHA.118.010641.
[6] I.F. van der Velpen, S. Feleus, A.S. Bertens, et al., Hemodynamic and serum cardiac markers and risk of cognitive impairment and dementia, Alzheimer Dement. 13 (4) (2017) 441–453, doi:10.1016/j.jalz.2016.09.004.
[7] K.S. Heffernan, J.A. Augustine, W.K. Lefferts, et al., Arterial stiffness and cerebral hemodynamic pulsatility during cognitive engagement in younger and older adults, Exp. Gerontol. 101 (2018) 54–62 Epub 2017 Nov 10, doi:10.1016/j.exger.2017.11.004.
[8] L. Buratti, G. Viticchi, L. Falsetti, et al., Thresholds of impaired cerebral hemodynamics that predict short-term cognitive decline in asymptomatic carotid stenosis, J. Cereb. Blood Flow Metab. 36 (10) (2016) 1804–1812, doi:10.1177/0271678X15613526.
[9] R.B. Nielsen, L. Egefjord, H. Angleys, et al., Capillary dysfunction is associated with symptom severity and neurodegeneration in Alzheimer's disease, Alzheimer Dement. 13 (10) (2017) 1143–1153, doi:10.1016/j.jalz.2017.02.007.
[10] L. Vinciguerra, G. Lanza, V. Puglisi, et al., Transcranial Doppler ultrasound in vascular cognitive impairment-no dementia, PLoS One 14 (4) (2019) e0216162, doi:10.1371/journal.pone.0216162.
[11] B. Sabayan, S. Jansen, A.M. Oleksik, et al., Cerebrovascular hemodynamics in Alzheimer's disease and vascular dementia: a meta-analysis of transcranial Doppler studies, Ageing Res. Rev. 11 (2) (2012) 271–277, doi:10.1016/j.arr.2011.12.009.
[12] C.M. Kim, R.L. Alvarado, K. Stephens, et al., Associations between cerebral blood flow and structural and functional brain imaging measures in individuals with neuropsychologically defined mild cognitive impairment, Neurobiol. Aging 86 (2020) 64–74, doi:10.1016/j.neurobiolaging.2019.10.023.
[13] M.J. Firbank, J. He, A.M. Blamire, et al., Cerebral blood flow by arterial spin labeling in poststroke dementia, Neurology 76 (17) (2011) 1478–1484, doi:10.1212/WNL.0b013e318217e76a.
[14] B. Yew, D.A. Nation, Alzheimer's Disease Neuroimaging Initiative, Cerebrovascular resistance: effects on cognitive decline, cortical atrophy, and progression to dementia, Brain 140 (7) (2017) 1987–2001, doi:10.1093/brain/awx112.

[15] S.E. Berman, L.R. Clark, L.A. Rivera-Rivera, et al., Intracranial arterial 4D flow in individuals with mild cognitive impairment is associated with cognitive performance and amyloid positivity, J. Alzheimer Dis 60 (1) (2017) 243–252, doi:10.3233/JAD-170402.
[16] J.N. Stember, K.L. Terilli, E. Perez, et al., Surface point cloud ultrasound with transcranial Doppler: coregistration of surface point cloud ultrasound with magnetic resonance angiography for improved reproducibility, visualization, and navigation in transcranial doppler ultrasound, J. Digit. Imaging (2020), doi:10.1007/s10278-020-00328-y.
[17] K. Gong, P. Han, G. El Fakhri, et al., Arterial spin labeling MR image denoising and reconstruction using unsupervised deep learning, NMR Biomed. (2019) e4224, doi:10.1002/nbm.4224.
[18] A. Strater, A. Huber, J. Rudolph, et al., 4D-flow MRI: technique and applications, RoFo 190 (11) (2018) 1025–1035, doi:10.1055/a-0647-2021.
[19] G. Pontone, M.G. Rabbat, The new era of computational fluid dynamics in CT angiography: far beyond the FFR number, JACC Cardiovasc. Imaging 10 (6) (2017) 674–676, doi:10.1016/j.jcmg.2016.08.001.
[20] J.K. Min, J. Leipsic, M.J. Pencina, et al., Diagnostic accuracy of fractional flow reserve from anatomic CT angiography, JAMA 308 (12) (2012) 1237–1245, doi:10.1001/2012.jama.11274.
[21] B.S. Ko, D.T. Wong, B.L. Norgaard, et al., Diagnostic Performance of transluminal attenuation gradient and noninvasive fractional flow reserve derived from 320-detector row CT angiography to diagnose hemodynamically significant coronary stenosis: an NXT substudy, Radiology 279 (1) (2016) 75–83, doi:10.1148/radiol.2015150383.
[22] K.M. Saqr, S. Rashad, S. Tupin, et al., What does computational fluid dynamics tell us about intracranial aneurysms? A meta-analysis and critical review, J. Cereb. Blood Flow Metab. (2019) 271678x19854640, doi:10.1177/0271678X19854640.
[23] J. Liu, Z. Yan, Y. Pu, et al., Functional assessment of cerebral artery stenosis: a pilot study based on computational fluid dynamics, J. Cereb. Blood Flow Metab. 37 (7) (2017) 2567–2576, doi:10.1177/0271678X16671321.
[24] L. Zhong, J.M. Zhang, B. Su, et al., Application of patient-specific computational fluid dynamics in coronary and intra-cardiac flow simulations: challenges and opportunities, Front. Physiol. 9 (2018) 742, doi:10.3389/fphys.2018.00742.
[25] H.S. Nam, F. Scalzo, X. Leng, et al., Hemodynamic impact of systolic blood pressure and hematocrit calculated by computational fluid dynamics in patients with intracranial atherosclerosis, J. Neuroimaging 26 (3) (2016) 331–338, doi:10.1111/jon.12314.
[26] A. Arzani, Accounting for residence-time in blood rheology models: do we really need non-Newtonian blood flow modeling in large arteries? J. R. Soc. Interface 15 (146) (2018), doi:10.1098/rsif.2018.0486.
[27] J.P. Mynard, D.A. Steinman, Effect of velocity profile skewing on blood velocity and volume flow waveforms derived from maximum Doppler spectral velocity, Ultrasound Med. Biol. 39 (5) (2013) 870–881, doi:10.1016/j.ultrasmedbio.2012.11.006.
[28] P.R. Rosenbaum, D.B. Rubin, The central role of the propensity score in observational studies for causal effects, Biometrika 70 (1) (1983) 41–55.
[29] A. Hayes, Introduction to Mediation, Moderation, and Conditional Process Analysis: A Regression-Based Approach, Guilford Press, New York, US, 2013.
[30] L. Lan, H. Liu, V. Ip, et al., Regional high wall shear stress associated with stenosis regression in symptomatic intracranial atherosclerotic disease, Stroke 51 (10) (2020) 3064–3073, doi:10.1161/STROKEAHA.120.030615.
[31] M. Boban, P. Crnac, A. Junakovic, et al., Blood flow velocity changes in anterior cerebral arteries during cognitive tasks performance, Brain Cogn. 84 (1) (2014) 26–33, doi:10.1016/j.bandc.2013.10.006.
[32] P. Scheel, I. Puls, G. Becker, et al., Volume reduction in cerebral blood flow in patients with vascular dementia, Lancet 354 (9196) (1999) 2137, doi:10.1016/S0140-6736(99)04016-7.
[33] E.D. Gommer, E.G. Martens, P. Aalten, et al., Dynamic cerebral autoregulation in subjects with Alzheimer's disease, mild cognitive impairment, and controls: evidence for increased peripheral vascular resistance with possible predictive value, J. Alzheimer Dis. 30 (4) (2012) 805–813, doi:10.3233/JAD-2012-111628.
[34] A.J. Wheaton, M. Miyazaki, Non-contrast enhanced MR angiography: physical principles, J. Magn. Reson. Imaging 36 (2) (2012) 286–304, doi:10.1002/jmri.23641.
[35] J.M. Wardlaw, C. Smith, M. Dichgans, Small vessel disease: mechanisms and clinical implications, Lancet Neurol. 18 (7) (2019) 684–696, doi:10.1016/S1474-4422(19)30079-1.
[36] L. Gustafson, E. Englund, H. Brunnstrom, et al., The accuracy of short clinical rating scales in neuropathologically diagnosed dementia, Am. J. Geriatr. Psychiatry 18 (9) (2010) 810–820, doi:10.1097/JGP.0b013e3181cdef7a.
[37] W.J.W. Bos, E. Verrij, H.H. Vincent, et al., How to assess mean blood pressure properly at the brachial artery level, J. Hypertens. 25 (4) (2007) 751–755, doi:10.1097/HJH.0b013e32803fb621.
[38] L.W.H. Lehman, M. Saeed, D. Talmor, et al., Methods of blood pressure measurement in the ICU, Crit. Care Med. 41 (1) (2013) 34–40, doi:10.1097/CCM.0b013e318265ea46.